$$+\exp[2\pi i\mathbf{X}\cdot(\mathbf{B}'_H+\mathbf{B}_T)]\sum_j \bar{f}_j\{\tfrac{1}{2}\varepsilon_j\exp(2\pi i\alpha'_j)$$

$$+\pi i\mathbf{B}'_H\cdot\Delta_j\exp(2\pi i\alpha_j)\cdot\exp[2\pi i\xi_{oj}\cdot(\mathbf{B}'_H+\mathbf{B}_T)]\}$$

$$+\exp[2\pi i\mathbf{X}\cdot(\mathbf{B}'_H-\mathbf{B}_T)]\sum_j \bar{f}_j\{\tfrac{1}{2}\varepsilon_j\exp(-2\pi i\alpha'_j)$$

$$+\pi i\mathbf{B}'_H\cdot\Delta_j\exp(-2\pi i\alpha_j)$$

$$\times\exp[2\pi i\xi_{oj}\cdot(\mathbf{B}'_H-\mathbf{B}_T)]\}\,.$$

Summing further over the unit cells, the first term leads to sharp main reflections, the second and third terms lead to sharp satellite reflections located at $\mathbf{B}_H\pm\mathbf{B}_T$, where $\mathbf{B}_H$ is a reciprocal lattice vector based on the reciprocal-cell edges of the subcell. The generalized atomic scattering factor is

$$\bar{f}_j(\tfrac{1}{2}\varepsilon_j\exp(-2\pi i\alpha'_j)+\pi i\Delta_j\cdot\mathbf{B}'_H\exp(-2\pi i\alpha_j) \qquad (12)$$

for reflections at $\mathbf{B}_H+\mathbf{B}_T$. For reflections at $\mathbf{B}_H-\mathbf{B}_T$ signs change in the exponent of the phase factors of the generalized atomic scattering factor.

Glossary of some more frequently used symbols

$\mathbf{a},\mathbf{b},\mathbf{c}$	Base vectors of the subcell.
$\mathbf{a}^*,\mathbf{b}^*,\mathbf{c}^*$	Base vectors of the reciprocal lattice based on the subcell.
Δ_{ps}	Displacement vector of the pth atom in the sth subcell from its average position ξ_p.
$\bar{f}_p$	Average atomic scattering factor of the pth atom.
ε_{ps}	Fractional increment of the atomic scattering factor of the pth atom in the sth cell.
$\mathbf{B}_H$	Reciprocal lattice vector of a main reflection.
$\mathbf{B}^a_H$	Reciprocal lattice vector of a difference reflection of the ath set.
β^a	Difference between $\mathbf{B}^a_H$ and $\mathbf{B}_H$.
Φ^a_s	Phase factor of the contribution from the sth subcell to a difference reflection of the ath set.
Ψ^a_p	Generalized atomic scattering factor for difference reflections of the ath set.
${}^aQ(\boldsymbol{\eta})$	Fourier transform of structure factors of reflections belonging to the ath set.
$U^a(\boldsymbol{\eta})$	Patterson function based on intensities of reflections of the ath set.

References

KOREKAWA, M. (1967). Habilitationsschift, Universität München.

GUINIER, A. (1963). *X-Ray Diffraction*, San Francisco and London: Freeman.

SMITH, J. V. & RIBBE, P. H. (1969). *Contrib. Min. Petrogr.* **21**, 157–202

Acta Cryst. (1973). A**29**, 127

Patterson Function of Plagioclase Satellites

BY K. TOMAN

Department of Geology, Wright State University, Dayton, Ohio, U.S.A.

AND A. J. FRUEH

Department of Geology and Institute of Materials Science, University of Connecticut, Storrs, Connecticut, U.S.A.

(*Received* 12 *May* 1972; *accepted* 14 *September* 1972)

The real and imaginary parts of Patterson functions based on '*e*' and '*f*' satellites were calculated. In '*e*' satellite maps, Patterson interactions involving cations are most prominent and permit relatively simple calculation of the amplitudes and phases of 26 displacement modulation waves. The deformation of the silicate chain, which is apparently one of the major features of the plagioclase superstructure, is shown in detail. The interpretation of the '*f*' satellite Patterson function is less straightforward, but it shows clearly that the associated displacements are of very small amplitude, directed along [02$\bar{5}$] and that they do not involve Na/Ca cations.

1. Introduction

In two earlier papers (Toman & Frueh, 1971; Toman & Frueh, 1972 henceforth referred to as TF1 and TF2) the nature of the plagioclase superstructure was examined by studying the statistical distribution of the intensities of satellite reflections. The chemical composition of the sample examined in these two papers corresponds to a plagioclase with 55% anorthite, and the results formulated there can be condensed as follows:

(*a*) The intensity distributions of '*e*' satellites (for terminology see Bown & Gay, 1958, or TF1) and of '*f*' satellites are qualitatively very different, suggesting that the '*e*' and '*f*' satellites are related to entirely different aspects of the superstructure.

(*b*) The anisotropy of the intensity distribution of '*e*' satellites and its variation with the square of the reciprocal vector suggests that the origin of '*e*' satellites is connected with the displacement by about 0·25–0·30 Å of atoms approximately parallel to the *b* axis.

Following these results, the study was extended by computing three-dimensional Patterson functions based exclusively on the satellite intensities previously used in our statistical studies (TF1, TF2). The interpretation of the Patterson functions is based on the concept of generalized atomic scattering factors derived in the preceding paper (Toman & Frueh, 1973, henceforth referred to as TF3).

2. The Patterson function based on '*e*' satellite intensities

The Patterson function of satellite intensities is defined in this paper as

$$U(\boldsymbol{\eta}) = \frac{1}{V}\sum_{H}^{s} I_H^s \exp\left(-2\pi i \boldsymbol{\eta} \cdot \mathbf{B}_H^s\right) \qquad (1)$$

where the summation is taken over reflections belonging to a particular set of satellites only, and where $\mathbf{B}_H^s$ is the corresponding reciprocal vector. In the case of '*e*' satellites,

$$\mathbf{B}_H^s = \mathbf{B}_H + \boldsymbol{\beta}^e$$

where $\mathbf{B}_H$ is the reciprocal lattice vector based on the unit cell of anorthite with $h+k$ odd and l odd (*b* reflections), and $\boldsymbol{\beta}^e$ is the vector showing the displacement of the reciprocal vectors of '*e*' satellites from '*b*' positions. In our case,

$$\boldsymbol{\beta}^e = -0{\cdot}062\mathbf{a}^* - 0{\cdot}051\mathbf{b}^* + 0{\cdot}219\mathbf{c}^* .$$

The intensities in one satellite pair (the intensity at $\mathbf{B}_H + \boldsymbol{\beta}^e$ is I_H^e, the intensity at $\mathbf{B}_H - \boldsymbol{\beta}^e$ is I_H^{-e}) are generally different, and because of Friedel's law we have

$$I_H^{-e} = I_H^e;$$

therefore, the Patterson function of '*e*' satellites is a complex function. According to the results in TF3, we expect that the Patterson function of '*e*' satellites will consist of convolutions of Fourier transforms of the generalized atomic factors centered at the end points of the average interatomic vectors. These convolutions (described in more detail in TF3) are generally complex, consisting of several positive and negative peaks and carrying information about displacements and/or substitutions of atoms in individual subcells. If we adopt the model of a modulated structure, they also carry information about phase relationships between waves modulating individual atomic sites involved in particular Patterson interactions.

In the case of '*e*' satellites of the plagioclase, the summation in (1) is restricted to the $\mathbf{B}_H$ vectors corresponding to '*b*' reflections only; therefore, each convolution placed at an end point of a corresponding interatomic vector is accompanied by identical convolutions displaced by $\frac{1}{2}(\mathbf{a}+\mathbf{b}+\mathbf{c})$ and by negative convolutions displaced by $\frac{1}{2}(\mathbf{a}+\mathbf{b})$ and $\frac{1}{2}\mathbf{c}$.

To simplify numerical calculations and to avoid extensive programming, instead of the function $U(\boldsymbol{\eta})^e$, functions

$$C(\boldsymbol{\eta}) = \frac{1}{2V}\sum_{H}^{e} (I_H^e + I_H^{-e}) \cos 2\pi\boldsymbol{\eta} \cdot \mathbf{B}_H$$

and

$$S(\boldsymbol{\eta}) = \frac{1}{2V}\sum_{H}^{e} (I_H^e - I_H^{-e}) \sin 2\pi\boldsymbol{\eta} \cdot \mathbf{B}_H$$

were calculated.

Based on these functions, the real part of the Patterson function is

$$\text{Re } U(\boldsymbol{\eta})^e = \cos 2\pi\boldsymbol{\eta} \,.\, \boldsymbol{\beta}^e C(\boldsymbol{\eta}) + \sin 2\pi\boldsymbol{\eta} \,.\, \boldsymbol{\beta}^e S(\boldsymbol{\eta}) \; ; \qquad (3)$$

similarly, the imaginary part of the Patterson function is

$$\text{Im } U(\boldsymbol{\eta})^e = \cos 2\pi\boldsymbol{\eta} \,.\, \boldsymbol{\beta}^e S(\boldsymbol{\eta}) + \sin 2\pi\boldsymbol{\eta} \,.\, \boldsymbol{\beta}^e C(\boldsymbol{\eta}) \,. \qquad (4)$$

For the numerical calculation of the Patterson function, more than 1500 independent satellite intensities were used, and the real and imaginary parts of the Patterson function were evaluated in slightly more than a quarter of a unit cell (based on an anorthite-like unit cell). Both the real and the imaginary parts of this Patterson function differ very substantially from the Patterson function based on the main (*a*) reflections. Patterson maps based on the main reflections of a plagioclase mainly show broad areas of high density corresponding to the superposition of many interaction vectors. On the other hand, Patterson maps calculated from '*e*' satellites are simpler and show a number of prominent, well separated peaks corresponding to cation–cation, cation–tetrahedral atom, and cation–oxygen interaction vectors (the identification of Patterson interactions in this paper is based on 'average' atom coordinates published by Phillips, Colville & Ribbe, 1971, for An_{28}).

The prominence of the interaction vectors involving cations shows the extraordinary role they play in determining '*e*' satellite intensities (see also TF2).

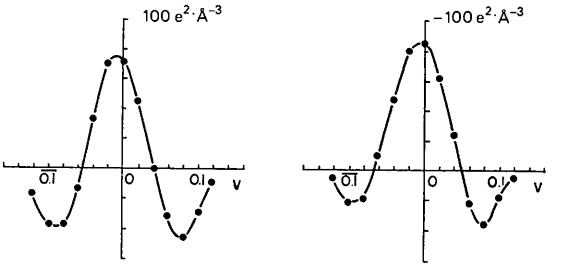

Fig. 1. Density values of Patterson function along a line going through centers of the main peak and of satellite peaks of a cation–cation interaction at $u=0{\cdot}525$, $v=0{\cdot}005$ and $w=0{\cdot}150$; (*a*) real part; (*b*) imaginary part. Density in e² Å^{-3}, v in fractions of *b* unit cell edge.

In the light of our treatment of difference reflections (see TF3), atomic interaction vectors here are not associated with simple convolutions of electron density functions (as is the case for crystals without a superstructure) but with convolutions of Fourier transforms of the generalized atomic scattering factors depending both on displacements of atoms in individual subcells from their average positions and on their substitutions. In our case, all these convolutions consist of three peaks arranged in a straight line, the 'central peak' and two 'satellite peaks'. Satellite peaks always have signs opposite to those of the 'central peak', which can be either positive or negative. The position vector of the central peak in the Patterson map corresponds to the interatomic vector of each particular Patterson interaction. The vectors connecting satellite peaks in convolutions do not differ significantly in different Patterson interactions, either in magnitude or in direction. The fact that these vectors have approximately the same direction for all Patterson interactions means that all atoms are displaced from their average positions approximately in the same direction. This result does not depend on any assumption about the nature of the superstructure.

2.1. Na/Ca *cation–cation interactions*

The most prominent features of Patterson maps based on '*e*' satellites are Patterson interactions corresponding to the Na/Ca cation–cation vectors. To illustrate this, Fig. 1 shows the variation of the density along a line going through the centers of the central peak and of both satellite peaks of a cation–cation convolution. A striking similarity is apparent between this function and R'_{pq} functions calculated in TF3 for different models of modulated structures (Figs. 8 and 9 in TF3).

The average direction of the line passing through the centers of both satellite peaks and of the central peak in cation–cation convolutions is $[07\bar{2}]$ (relating to the anorthite-like unit cell) indicating the direction of the displacement of the cations from their mean positions. The angle between this direction and the *b* axis is approximately 20°. In the volume of the Patterson space examined in this study ($0 \le x \le 1$, $0{\cdot}10 \le y \le 0{\cdot}60$, $0 \le z \le 0{\cdot}50$) there are 4 cation–cation interactions represented by prominent peaks on the maps of both the real and the imaginary parts. To be able to proceed further with the analysis, we must accept certain assumptions about the nature of the superstructure.

Let us assume that the plagioclase superstructure is a modulated structure, where the exact position of each atom in a given site is determined by a displacement modulation wave. Similarly, we assume that the occupation of each atomic site is determined by a density modulation wave. From the geometrical arrangement of the satellite reflections, it may be assumed that the wave vectors of all modulation waves in the structure are equal to $\boldsymbol{\beta}^e$. No assumptions are made about the wave form of the modulation waves, but it may be assumed that their amplitudes and phases may be different, but that their wave form is identical or very similar. Further, we accept the proposition of Korekawa & Jagodzinski (1967) that the phase of the modulation waves related to the atomic sites differing by $\frac{1}{2}\mathbf{c}$ or by $\frac{1}{2}(\mathbf{a}+\mathbf{b})$ differ by π, and that the atomic sites related by a vector $\frac{1}{4}(\mathbf{a}+\mathbf{b}+\mathbf{c})$ have identical phases of their modulation waves (related to an anorthite-like unit cell). Therefore, it remains to calculate the amplitudes and phases of the modulation waves related to all independent atomic sites of our plagioclase structure.

A simple computation based on equation (9) in TF3 shows that the phase difference $\Delta\alpha$ between two modulation waves involved in a Patterson interaction can be calculated from maximum densities in the central peaks in the real and imaginary parts of the Patterson function (m_r and m_i respectively). For almost any form of modulation wave we have:

$$\tan \Delta\alpha = m_i/m_r \, .$$

In the application of this formula we assume that the phase of the displacement modulation wave associated with the cation in 000 position is equal to zero. The phase calculation for the displacement modulation wave of the 00*c* cation site is listed in Table 1. (Megaw's notation of the atomic sites in feldspars is used throughout this paper – Megaw, 1956.)

Table 1. *Displacement modulation waves of all independent atoms in plagioclase superstructure*

'Maximum' column shows the maximum absolute value of the central peak. Phase of the displacement wave is in π.

Atom	Position	Maximum e^2 Å^{-3}	Displacement waves Amplitude Å	Phase
Na/Ca	000	122	0·6	0·00
	00*c*	122	0·6	0·28
T_1	0000	91	0·4	0·08
	000*c*	91	0·4	0·20
T_1	*m*000	114	0·5	0·11
	*m*00*c*	114	0·5	0·19
T_2	0000	82	0·3	0·91
	000*c*	75	0·3	1·37
T_2	*m*000	89	0·3	1·12
	*m*00*c*	88	0·3	1·16
$O_A(1)$	0000	64	0·5	1·43
	000*c*	66	0·5	0·92
$O_A(2)$	0000	42	0·2	0·97
	000*c*	37	0·2	1·14
O_B	0000	18	0·1	0·46
	000*c*	18	0·1	0·82
O_B	*m*000	18	0·1	1·39
	*m*00*c*	34	0·2	0·95
O_C	0000	66	0·4	0·00
	000*c*	68	0·5	0·28
O_C	*m*000	69	0·5	1·96
	*m*00*c*	67	0·5	0·28
O_D	0000	38	0·2	0·14
	000*c*	42	0·2	0·16
O_D	*m*000	31	0·2	0·20
	*m*00*c*	33	0·2	0·07

The determination of the displacements of cations from their average positions is slightly more difficult and less reliable, because it depends on assumed wave forms. Fig. 4 (Appendix) shows the dependence of the separation of satellite peaks on the amplitude of the modulation wave and on its form. The calculation was performed for models where both displacement modulation waves involved in a Patterson interaction have the same amplitude. Comparing these results with the observed separation of satellite peaks for cation–cation interactions, which on our Patterson maps is 2·18 Å, we obtain 0·57–0·63 Å for the amplitudes of cation modulation waves.

2.2. *Cation–T-atom and cation–oxygen vectors.*

Altogether, 48 interaction vectors of this type can be identified in a quarter of a Patterson cell. Each of them is associated with a convolution similar in shape to the convolutions described in more detail in § 2. Lines connecting the satellite peaks in each convolution have orientations identical within narrow limits, showing that all the atoms in the structure are displaced approximately in the same direction. Most Patterson interactions here have significant imaginary parts, and therefore phases associated with the displacement modulation waves involved were calculated in the same way as described in the preceding section for cation–cation vectors.

To determine the amplitudes of the modulation waves of *T*-atoms and of oxygen atoms from Patterson interactions involving cations, it is possible to use a procedure similar to that employed in the previous section to determine the amplitude of cation displacement modulation waves. However, this method is not very efficient in this case, because the exact values of the separation of the satellite peaks frequently cannot be determined for these rather weaker convolutions (especially if partial overlaps occur). As is shown in the Appendix, the maximum density of the central peak of a Patterson interaction depends on the displacement amplitudes of both modulation waves involved in it (Fig. 5). This makes it possible to determine the amplitudes of the displacement modulation waves of all atoms from the amplitude of the cation modulation wave (determined in the previous paragraph) and from maximum densities in the central peaks of Patterson interactions involving cations. A further check of amplitudes determined by using this method is possible by comparing their weighted average with the average displacement obtained in our statistical study (TF2). The weighted average of amplitudes obtained from Patterson peaks (weights proportional to the squares of the atomic numbers of the atoms involved) is 0·39 Å for a 'square' wave and 0·42 Å for a simple cosine wave. This corresponds to an average displacement of 0·35 Å for the square wave and 0·27 Å for a simple cosine wave, which compares well with the statistical result, 0·25–0·30 Å, obtained in TF2 without any assumptions. The amplitudes of displacement modulation waves of all 26 independent atomic sites in the anorthite-like cell as determined from the Patterson peaks (simple cosine waves), together with their phases, are listed in Table 1. The amplitudes are indicated with one significant figure accuracy, which reflects both the difficulties inherent in extracting quantitative information from Patterson interactions, and the semiquantitative nature of these figures. Even with this limitation, these data are useful, because they reveal the periodic distortion of the silicate chain discussed in § 4, and they provide information for determining the phases of Fourier terms in an electron-density calculation based on satellite reflections; this calculation is the next logical step in the investigation of the plagioclase superstructure. For atoms in sites related by translations $\frac{1}{2}\mathbf{c}$ or $\frac{1}{2}(\mathbf{a}+\mathbf{b})$, the amplitudes of the modulation waves are assumed to be equal and the phase shifted by π; for sites related by translations $\frac{1}{2}(\mathbf{a}+\mathbf{b}+\mathbf{c})$, both the phases and the amplitudes of the modulation waves are assumed to be equal. Each entry in Table 1 was compiled from evaluation of two Patterson interactions involving atoms related to the same basic sites but displaced by $\frac{1}{2}\mathbf{c}$ or $\frac{1}{2}(\mathbf{a}+\mathbf{b})$ or $\frac{1}{2}(\mathbf{a}+\mathbf{b}+\mathbf{c})$. When the above-mentioned Korekawa–Jagodzinski phase conditions were applied, they led to very similar phase values.

3. Patterson function based on '*f*' satellite intensities

The Patterson function based on '*f*' satellite intensities was calculated in much the same way as for the Patterson function based on '*e*' satellite reflections,

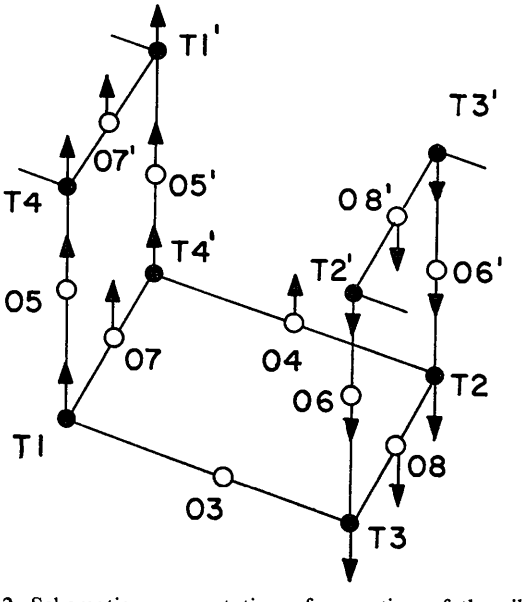

Fig. 2. Schematic representation of a portion of the silicate chain, showing displacement of atoms. Numbering of atoms is identical to that in Table 2. Arrows indicate schematically the directions and magnitudes of displacements.

described in § 2. Maps corresponding to the real and the imaginary parts were calculated, using about 1600 independent intensities. Because the '*f*' satellite intensities from our sample are very weak, Patterson functions based on them probably contain more spurious features than the Patterson function of '*e*' satellites. On '*f*' satellite maps, Patterson density is largely concentrated in three regions (close to $u=0{\cdot}0$, $0{\cdot}5$ and $0{\cdot}75$), where it forms systems of extended, parallel streaks situated perpendicular to the $[02\bar{5}]$ direction. It is interesting to note that streaks in the imaginary part of the Patterson function interpose positive and negative streaks in the real part.

When comparing the positions of these streaks with a set of calculated interatomic vectors, we see a striking difference between the '*f*' and the '*e*' satellite maps. In the case of the '*f*' satellite maps, areas of high Patterson density correspond not to interatomic vectors involving the Na/Ca cations, but to interatomic vectors involving some *T*-atoms and some oxygen atoms. At present we are not able to give a detailed interpretation of the '*f*' satellite Patterson function as we have in the case of '*e*' satellites. The most likely interpretation of streaks observed there is that they correspond to overlapping convolutions of Fourier transforms of generalized atomic scattering factors, where atoms are displaced by a very small distance in the $[02\bar{5}]$ direction. From the density of the Patterson function we estimate that the displacements involved are 5–10 times smaller than those associated with '*e*' satellites. The direction of displacements derived here is in reasonable agreement with the direction of the displacement found by intensity statistics in TF2, where $[01\bar{1}]$ was established for the direction of the displacements.

4. Discussion

In summarizing the results derived above on the Patterson functions based on '*e*' and '*f*' satellite intensities, we find that one problem which can be partially answered concerns the deformation of silicate chains in the superstructure. The general direction of displacement of all atoms in the plagioclase superstructure due to modulation waves causing '*e*' satellites is $[07\bar{2}]$. Assuming some simple form of the modulation wave, it is possible to calculate the magnitudes of the displacements of atoms in one particular subcell of the superstructure (the anorthite-like unit cell) from information in Table 1. Assuming a simple cosine wave with wave vector $\boldsymbol{\beta}^e$, the results of such a calculation are shown in Table 2 for atoms in a subcell where cation 000 has its maximum positive displacement. Fig. 2 illustrates schematically how individual atoms in a silicate chain are affected by these displacements. Silicate rings oriented parallel to the *b* axis are alternately lifted and lowered in the $[07\bar{2}]$ direction, whereas rings perpendicular to the *b* axis are twisted approximately around an axis going through oxygen atoms O_B $00i0$ and O_B *mzic*, Alternatively, the deformation can be expressed as an alternate lifting and lowering of sheets of atoms [approximating the $(10\bar{1})$ planes] containing silicate rings parallel to the *b* axis.

Fig. 3 illustrates schematically the variation of the magnitude and direction of these displacements through different subcells of the superstructure 'carried' by a modulation wave of wave vector $\boldsymbol{\beta}^e$. It is important to note that the amplitudes and phases of the displacement modulation waves, determined purely by diffraction methods without the use of any chemical evidence, compose themselves into a plausible, coherent picture of a periodic deformation of the silicate chains.

Deformations of the silicate chains in the structure are accompanied by large displacements of cations (see Table 1). At present it is impossible to discuss a causal relationship between displacements of cations and deformations of silicate chains because two basic pieces of information are lacking: one is the evidence

Table 2. *Displacement of atoms shown in a portion of the silicate chain of plagioclase in Fig.* 3

Atom	Position	Displacement	Atom	Position	Displacement
*T*1	T_1 $00i0$	+0·3 Å	05	O_C 0000	+0·4 Å
*T*1′	T_1 $000c$	+0·2	05′	O_C $000c$	+0·4
*T*2	T_1 *mzic*	−0·5	06	O_C *mz*00	−0·5
*T*2′	T_1 *mz*00	−0·5	06′	O_C *mzic*	−0·4
*T*3	T_2 $00i0$	−0·3	07	O_D $00i0$	+0·1
*T*3′	T_2 $000c$	+0·1	07′	O_D $000c$	+0·2
*T*4	T_2 *mz*00	+0·3	08	O_D *mzic*	−0·1
*T*4′	T_2 *mzic*	+0·3	08′	O_D *mz*00	−0·2
O3	O_B $00i0$	0·0			
O4	O_B *mzic*	+0·2			

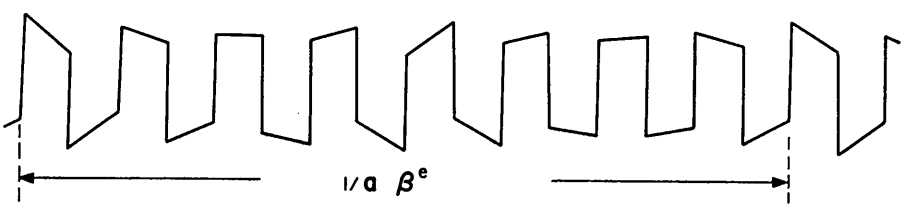

Fig. 3. Schematic diagram of silicate chain in plagioclase superstructure showing modulation of displacements of rings.

as to how cations are ordered in the superstructure. From a previous study (see TF1), we have an indication that they are ordered in some way, but we have not as yet been able to derive from convolutions on Patterson maps the way in which they are ordered. The second piece of information still needed is the knowledge of the 'average' atom coordinates in a plagioclase of An_{55} composition.

At present, we know how individual atoms are displaced from their average positions, but without knowledge of the coordinates corresponding to the 'average' positions, it is impossible to calculate interatomic distances in individual subcells and their change owing to modulation.

Obviously, much more work is needed before the plagioclase superstructure will be reasonably well understood. First, it is necessary to calculate the 'average' structure from structure amplitudes of the '*a*' reflections of our crystal; second, it is desirable to calculate Fourier maps based on '*e*' satellite amplitudes. Phases necessary for the evaluation of these maps can be derived from information given in this paper on the displacement modulation waves. As shown in TF3, these maps will show the Fourier transforms of the generalized atomic scattering factors, which can be interpreted much more easily than their convolutions studied in the present paper. These Fourier maps should ultimately provide information about the displacements and occupations of atomic sites in the structure derivable by X-ray diffraction. Further, they will provide a basis for a rigorous check of the validity of the structure model – a comparison between calculated and observed satellite intensities.

Another question which may be discussed in part, at least, is the mutual relationship of '*e*' and '*f*' satellites. The origin of '*e*' satellites is fairly well understood; they are connected with the displacements of cations, *T*-atoms and some of the oxygen atoms in the $[07\bar{2}]$ direction by distances ranging from 0·1 to 0·6 Å. The origin of '*f*' satellites, on the other hand, is less well understood, but we know that they are related to additional small (just a few hundredths of an Å) displacements of some of the *T*-atoms and oxygen atoms (but not the cations) in the $[02\bar{5}]$ direction. The wavelength of the modulation waves associated with '*f*' satellites is half of the wavelength of the modulation waves associated with '*e*' satellites, but the direction of their wave vectors is identical.

Finally, mention should be made of two aspects of '*e*' satellite Patterson maps which were consistently observed, but which we do not attempt to interpret here as the interpretation would depend too greatly on additional assumptions and because we believe that the features to which they relate may be elucidated in a less ambiguous way from Fourier maps.

One of the aspects is the asymmetry of the vector density of 'satellite peaks' observed in all convolutions. (For cation–cation convolutions, see Fig. 1.) This may be related to Na/Ca order, but more definite conclusions depend largely on the assumed wave form of the modulation waves. Another aspect is the lack of exact agreement of the coordinates of maxima of 'central peaks' derived from the real and imaginary parts of the Patterson function. The slight misplacement of maxima which is observed on all cation–*T*-atom and cation–oxygen convolutions but not on cation–cation convolutions, may be related to small differences in wave forms of individual modulation waves, which seems to be a prerequisite if the pattern of Al/Si order were also to be modulated.

The support of this work by the National Science Foundation (GA 35246) is gratefully acknowledged.

APPENDIX

Using equation (9) from TF3, functions R'_{pq} were calculated for different models of modulated structures, where the form of the displacement modulation wave was either a simple cosine wave or a 'square' wave (composed of 5 cosine terms). Functions ϱ'_p and ϱ'_q were represented by $\exp(-kx^2)$, with $k = 4$ Å, which was derived from the widths of Patterson peaks ob-

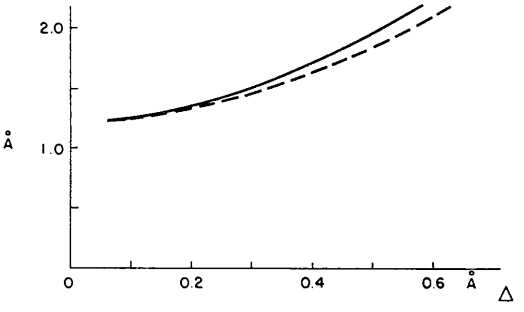

Fig. 4. Variation of satellite peak separation with the amplitude of both displacement modulation waves involved in the interaction. Solid line, square wave; broken line, cosine wave.

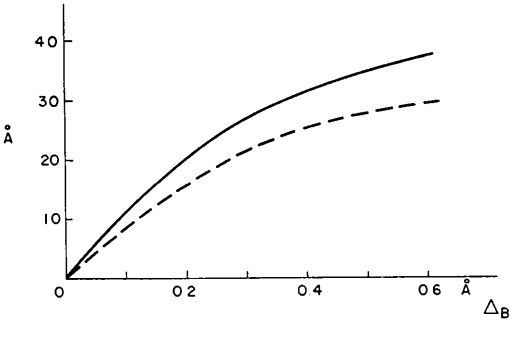

Fig. 5. Maximum density value in central peak of a Patterson interaction, where one displacement modulation wave has constant amplitude (0·55 Å) and the amplitude of the second modulation wave varies from 0 to 0·6 Å.

served on our maps. Fig. 4 shows the variation of the 'satellite peak' separation with the amplitude of the displacement. Both modulation waves involved in the Patterson interaction have the same amplitude and phase. In Fig. 5, the maximum density in the central peak is shown for the Patterson interaction of two displacement modulation waves with equal phase but with different amplitudes. The amplitude of one wave is constant (0·55 Å); the amplitude of the other modultion wave varies from 0 to 0·6 Å.

Note added 29 *August* 1972. The least squares refinement of atomic coordinates based on measured '*a*' reflections from this sample has been completed and published elsewhere. It produced coordinates that in some cases (Na/Ca cations) differed substantially from those given by Phillips *et al.* (1971) but these differences do not effect the conclusions reached in this paper.

References

BOWN, M. G. & GAY, P. (1958). *Z. Kristallogr.* **111**, 1–14.

KOREKAWA, M. & JAGODZINSKI, H. (1967). *Schweiz. Miner. Petrogr. Mitt.* **47**, 269–278.

MEGAW, H. D. (1956). *Acta Cryst.* **9**, 56–60.

PHILLIPS, M. W., COLVILLE, A. A. & RIBBE, P. H. (1971). *Z. Kristallogr.* **133**, 43–65.

TOMAN, K. & FRUEH, A. J. (1971). *Acta Cryst.* B**27**, 2182–2186.

TOMAN, K. & FRUEH, A. J. (1972). *Acta Cryst.* B**28**, 1657–1662.

TOMAN, K. & FRUEH, A. J. (1973). *Acta Cryst.* A**29**, 121–127.

Acta Cryst. (1973). A**29**, 133

The Phase Function: New Developments in the Symbolic-Addition Procedure

BY CLAUDE RICHE*

Laboratoire de Cristallochimie, Faculté des Sciences, Tour 44, *quai Saint Bernard,* 75-*Paris* 5*ème, France*

(*Received* 21 *September* 1972; *accepted* 8 *October* 1972)

A modification of the symbolic-addition procedure, based on the introduction of a 'phase function', is proposed. This function which determines the numerical values of the symbols, enables one to select rapidly the best solution from a large number of possible ones. Examples of non-centrosymmetric structures solved by this method are given here.

Introduction

It is well known that the most critical part of solving non-centrosymmetric structures by direct methods lies in the determination of a starting set of numerical phases. The number of such phases increases with the complexity of the structure (Germain & Woolfson, 1968).

Karle and Karle who have demonstrated the power of these methods have developed a successful procedure using symbols (Karle & Karle, 1966). The main difficulties in using this procedure are:

(*a*) in the first step, single indications of phases from equation (1) must be accepted

$$\varphi_{\mathbf{H}} \simeq \varphi_{\mathbf{K}} + \varphi_{\mathbf{H}-\mathbf{K}} \text{ (Cochran, 1955),} \qquad (1)$$

(*b*) considerable care must be applied in the use of equation (2)

$$\varphi_{\mathbf{H}} \simeq <\varphi_{\mathbf{K}} + \varphi_{\mathbf{H}-\mathbf{K}}>_{\mathbf{K}} \text{ (Karle \& Karle, 1966)} \qquad (2)$$

(*c*) determination of the numerical values of the symbols.

Starting with numerical phases instead of symbols, the multisolution approach (Germain & Woolfson, 1968; Germain, Main & Woolfson, 1970, 1971) seems to be the most practical 'computer-based' method but is however limited in view of computational cost and, in unfavourable cases, of the number of Fourier syntheses to examine.

The need for a safe procedure to assign numerical values to the symbol used in the symbolic-addition method led us to the formulation of an appropriate test called 'the phase function' (Riche, 1970). We showed that the most probable combination of phases $\{\varphi_i\}$ belonging to a set of high $|E|$ values is given by the maximum of relation (6).

Later on, Schenk (1971) used some practical tests to select numerical values for the symbols. One of them (Q function) could be related to the phase function.

We recall briefly how we formulated relation (6) in § I. Use of the phase function and the change it produces in the symbolic-addition method is shown in § II. The practical procedure for phase determination is described in § III. In § IV results are discussed.

* Present address: Institut de Chimie des Substances Naturelles du C.N.R.S. 91, Gif sur Yvette, France.